Hindawi
Geofluids
Volume 2022, Article ID 9745733, 12 pages
https://doi.org/10.1155/2022/9745733

Research Article

Shearing Performance of Natural Joints with Different Roughnesses under Direct Shearing Tests

Yang Zhang,[1] Jinliang Song,[2] Dawei Hu,[2] Yuzhang Liu,[1] and Fujian Zhou[1]

[1]*China University of Petroleum-Beijing, 18, Fuxue Road, Changping District, Beijing, China 102249*
[2]*State Key Laboratory of Geomechanics and Geotechnical Engineering, Institute of Rock and Soil Mechanics, Chinese Academy of Sciences, Wuhan, Hubei 430071, China*

Correspondence should be addressed to Jinliang Song; songjinliang12345@163.com

Received 17 January 2022; Accepted 7 March 2022; Published 26 March 2022

Academic Editor: Yu Zhao

Roughness is one of the major characteristics of natural fracture in hydrocarbon and geothermal reservoirs, which has a significant influence on the activation of fractures during hydraulic stimulation. The main purpose of this study is to investigate the effect of different roughnesses and high normal stresses on shear behaviors of rock joints. To do this, replicas of natural rock joint surfaces were constructed using the 3D optical scanning and 3D rigid engraving technique. Direct shear tests were performed on rock joint replicas with three joint roughness coefficient (JRC) indices (i.e., 1.42, 4.98, and 7.96) at two high normal load conditions (i.e., 15 and 30 MPa). The results show that the shear strength dependence on surface roughness is similar at normal stresses of 15 and 30 MPa. In addition, JRC-JCS shear strength criterion can reasonably describe the peak shear strengths that obtained from experimental curves, and the peak shear stresses have a positive correlation with JRC values at both normal stresses. Moreover, at normal stresses of 15 and 30 MPa, the shearing mechanism of joints with different JRC values is asperity shearing off. Results also show that the friction coefficient of joint surface increases as joint roughness increases, and higher normal loads may lead to a decrease of apparent cohesion, which weakens the residual strength during the slip. The results of this study improve insight into the natural fracture activation behavior during hydraulic fracturing.

1. Introduction

Hydraulic fracturing is successfully applied to improve the reservoir permeability, which has become a key technology of unconventional reservoir development [1, 2]. To get the long-term oil/gas/geothermal production from the reservoir, a mass of fracturing fluid and proppants are injected into the reservoir, so that the fracturing fluid can create complex rock fracture networks. To date, many studies have shown that the activation of natural fractures has significant influence on the propagation of hydraulic fractures and associated flow characteristics, especially the friction coefficient, which is closely related to the roughness of natural fracture surface, and has a strong influence on the interaction between the hydraulic fractures and the natural fractures [3–5]. During hydraulic fracturing, the natural fractures are likely to be activated under the shear stress, according to the Coulomb–Mohr failure criterion, and the effective normal stress, friction coefficient, and cohesion of the natural fractures are the main factors in determining the failure envelope and causing fracture activation. Therefore, it is of great significance to study the shear performances of joints with different roughnesses under different normal stresses.

The development of joints has a significant effect on the degradation of strength of the natural rock masses, and it is considered as an indicator to determine the stability of rock mass engineering [6–9]. Some researchers have focused on the studies of rock joints shear behavior in the past decades [10–14]. Generally, the shear mechanical properties of the tested surfaces are dominantly controlled by surface morphology of rock joints, in situ pressure, contact state, and filling materials. For commonly studied rock joints with well matching and without filling materials, the applied normal stress and roughness of the joints are dominant factors [15].

The joint surface roughness is considered as the key factor that affects the shear strength of the rock joints, and

many researchers have done a lot of researches on determining the roughness of the joints. Barton and Choubey first proposed the concept of joint roughness coefficient (JRC) through a large number of experiments, and the JRC was obtained on the basis of 10 two-dimensional (2D) profiles of the joint [16]. Based on this method, subsequent researchers proposed statistical parameter method [17–19] and fractal dimension method [20–23] to quantitatively describe the roughness of joint surface. Experimental and numerical direct shear tests were commonly carried out to characterize the relationship between roughness and shear strength at different normal load conditions, and the damage and scale effect of shear mechanical properties of nonpenetrating and penetrating jointed rock mass were also investigated [24, 25]. However, the applied normal stresses on joint surfaces are usually low (i.e., <3 MPa) in previous studies [15, 26–28]. In fact, the normal stresses acting on fault surfaces in deep underground are much higher; thus, laboratory experiments working on friction of joint surfaces require to consider higher normal stresses, e.g., >10 MPa.

During experimental study of natural rock joints, it is necessary to keep the joint surface morphological characteristics unchanged, but it is impossible to have absolutely two identical natural joint surfaces; therefore, the systematic experimental research is limited by insufficient joint samples with the same natural surface morphology. Now, the main methods of replicating joint specimens include tensile fractures [15, 29, 30], sawn flat joints with regular surfaces [27, 31, 32], and silicon casts of natural or stylized joints [28, 33, 34]. However, these methods may lead to objective errors in experimental results and increased time consumption in the preparation of specimens. For instance, the artificial joint samples generated by tensile fractures are random, and rock samples will be damaged in the loading process, which will affect the results of subsequent tests. Moreover, joint-casting methods using similar materials cannot be completely consistent with those of natural rock mass. Thus, a new production method for natural rock joints is required to overcome the present difficulty by replicating natural joint specimens to promote study of their mechanical properties.

In recent years, in geology, optical scanning methods have successively obtained digitized morphology of slip surfaces in faults and enabled high-quality and high-precision measurements on fault surfaces; thus, the major features of fault roughness can be observed [35, 36]. As an alternative, combining 3D optical scanning and 3D rigid engraving technique is a good means to replicate joint specimens with the same natural morphology [37]. The 3D optical scanning measurement is regarded as a nondestructive and high-precision technique, which can rapidly capture natural joint morphology, and then, digitized natural joint can be reconstructed in postprocessing software. The 3D rigid engraving is a good approach to produce joints with the same morphology of natural joint surfaces, and the original rock can be taken from the same outcrop in engineering field; then, based on digitization data of natural joint surfaces from 3D optical scanning, batch engraving production of artificial natural joints can be fabricated. Thus, the specimens with the same lithology, surface morphology and mechanical properties as the natural joints can be prepared repeatedly in large quantities, and the shear tests of the specimens manufactured by the above method can truly and accurately reflect the shear mechanical properties of the natural rock joints.

In this study, the 3D optical scanning and 3D rigid engraving were used for batch production of rock joints with different roughnesses for shearing tests. The optical scanning instrument was utilized to digitize 3D surfaces of natural rock joints from downhole cores at the underground depth of 6500-7000 m, and representative joints with three different JRC values (i.e., 1.42, 4.98, and 7.96) were selected for 3D rigid engraving. In this way, rock joint replicas with the same natural joint morphology were manufactured, and then, direct shear tests were performed at two normal stresses (i.e., 15 and 30 MPa). The failure characteristics of the joint surfaces with different rugosities were studied according to the strength evolution, surface morphology, and deformation features.

2. Test Materials and Reconstruction of Natural Rock Joints

2.1. Sampling Materials. A large volume of sandstone outcrop from Keshen block was selected for subsequent experimental works, the XRD was conducted to investigate its mineralogical composition, and samples were first crushed into small pieces and then grounded in a XPMΦ120 × 3 grinding miller (Weiming Mechanical Equipment Ltd., Jiangxi, China) for 20 min to obtain powder sample with particle sizes of <20 μm. Diffraction patterns were then obtained in a D8 Advance X-ray diffractometer (Bruker Inc., Germany) equipped with a Cu-Kα radiation at 60 kV and 80 mA, a continuous scan range of 2°-60° 2θ (where 2θ is the diffraction angle), and a scan rate of 1.0° 2θ/min. The quantitative mineralogy analysis from XRD experimental results is shown in Table 1.

The mechanical parameters of the used sandstone were further tested, the RMT-150C servo test system, which consisted of the main engine, the hydraulic system, the servo control system, and a digital controller with system software, was used to carry out uniaxial compression experiments on three cylindrical specimens with dimensions of 25 and 50 mm in diameter and height to determine the uniaxial compressive strength (UCS), elastic modulus (E), and Poisson's ratio (ν). The maximum vertical and horizontal loads of the RMT-150C servo test system were 1,500 and 500 kN, respectively, the load control rates ranged from 0.01 to 90 kN/s, and the deformation control rates varied from 0.0001 to1 mm/s. The mean values of UCS, E, and ν were regarded as the basic mechanical parameters of the studied sandstone. Through the uniaxial compression test, the mechanical parameters of the studied sandstone were obtained, and the UCS, E, and ν were 95.60 MPa, 23.74 GPa, and 0.25, respectively.

2.2. 3D Optical Scanning of the Original Rock Joint. The key procedures for replicating the natural rock joints include (1) the digital surface geometries of natural joints obtained by

Table 1: Mineralogical composition of the studied sandstone.

Mineral (wt.%)							
Quartz	Orthoclase	Albite	Calcite	Dolomite	Pyrite	Chlorite	Illite
13.3	0.3	2.5	14.6	53.9	0.37	3.5	11.5

the 3D optical scanning instrument; (2) batch production of the same natural rock joints manufactured by the 3D rigid engraving technique; and (3) comparison of the precision between natural joint surfaces and joint replicas.

The individual operating steps for acquiring geometry of the original rock joints involved the following:

(1) Scanning the morphologies of natural joints. Applying a 3D optical scanner to scan and record the natural rock joints of nine batches of downhole cores in the Keshen block, Tarim Basin, Korla, Xinjiang, China, and the scanning objects were mainly focused on the semifilled and unfilled natural joints, and the original sizes of natural joint surfaces were almost within 60 × 100 mm (width × length), to unify subsequent 3D rigid engraving and shear tests, the square with side length of 50 mm in the middle of each scanning region was selected as the research object. In this study, a portable 3D scanner with spatial resolution of 0.05 mm was utilized to scan sandstone joints. The representative digital 3D points cloud with (x, y, z) positions of the joint surfaces is shown in Figure 1

(2) The optimization and fusing of point cloud data. The synthesized point cloud data was obtained by using postprocessing software within the scanning system to optimize and fuse the point cloud data. The number of points of the obtained point cloud was not less than 400 in every square centimeter. The resultant data was imported into Geomagic Studio software (Raindrop Geomagic, Inc., Morrisville, NC, USA) to encapsulate the resultant mesh surface. Each mesh surface consisted of numerous triangular meshes with side of 0.5 mm. Finally, by deleting the noise data outside the joints, the reconstructed digital images were obtained which were completely consistent with the original rock joints

(3) The extraction of 2D profiles. After the scanning, we extracted nine 2D profile lines of a joint along the shearing direction and calculated its Z_2, and the JRC values for each joint along with the given shearing direction were estimated according to the empirical relationship between the JRC index and the Z_2 index [19], as shown in Equation (1). Three different JRC indices (i.e.,1.42, 4.98, and 7.96, respectively) which totally accounted for more than 75% of all the scanned natural joint surfaces were determined to adopt for subsequent experiments

$$Z_2 = \left[\frac{1}{L}\sum_{i=1}^{N-1}\frac{(z_{i+1}-z_i)^2}{x_{i+1}-x_i}\right]^{1/2} \quad (1)$$

$$L = \sum_{i=1}^{N-1}(x_{i+1}-x_i) \quad (2)$$

$$JRC = 32.2 + 32.47 \lg Z_2 \quad (3)$$

where Z_2 is the root mean square of the first derivative of the profile, the values (x_i, z_i) and (x_{i+1}, z_{i+1}) represent the adjacent coordinates of the profile separated by the sample interval Δx, N is the number of measurement points, and L is the nominal length of the profile.

(4) Establishing a mirroring surface based on the joint's acquired digital surface by way of reversing the plus and minus signs of a point's Z value, thus three couples of upper and lower digital surfaces were prepared for 3D engraving and shear tests

2.3. 3D Rigid Engraving of the Original Rock Joint. From our experience of engraving work for various rocks, the 3D rigid engraving method may not be appropriate for every kind of rock, for instance, granite is a crystalline rock with low porosity; hence, the cutter has difficulties in breaking the cohesion between grains, resulting in the poor quality of engraved surfaces. However, for the studied sandstone, which has a much higher porosity, it is formed by cementing small mineral particles, and cohesion among mineral particles is relatively small; hence, the rotating cutter can easily grind off extra portions in the block and introduce negligible damages to the engraved surface.

In this engraving work, based on digitized natural joints by the aforementioned 3D scanning, the computerized numerical control (CNC) engraving machine was used to carve natural joints of original rock blocks in the laboratory. The engraving machine mainly comprised of control system, main axle, work platform, and shield (Figure 2). The applied maximum power of main axle was 5.5 kW, and $X/Y/Z$-axis positional accuracy was 0.02 mm, which fully met the requirements of engraving work in this study.

A large block obtained from the sandstone outcrop was cut into many small blocks with the dimensions of 50 × 50 × 28 mm (length × width × height) for engraving. The specific operation steps were as follows:

(1) Making engraving paths. The surface information of the focused areas was transformed into the engraving paths of upper and lower surfaces that could be recognized by the engraving machine through a 3D

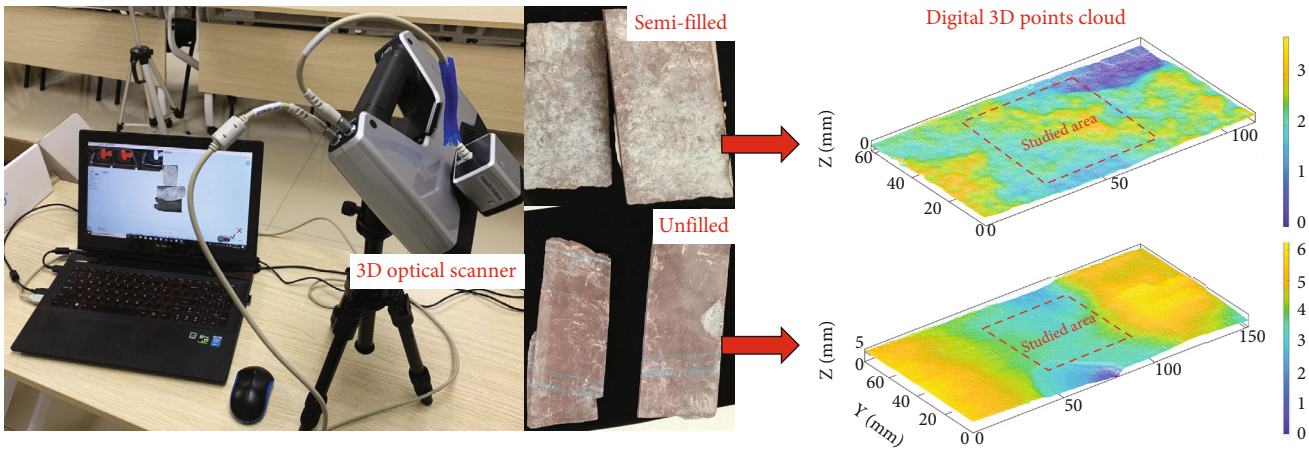

Figure 1: Basic process for acquiring the digital geometry of natural rock joints: (a) 3D optical scanner; (b) selected natural rock joints; (c) acquired digital 3D points cloud.

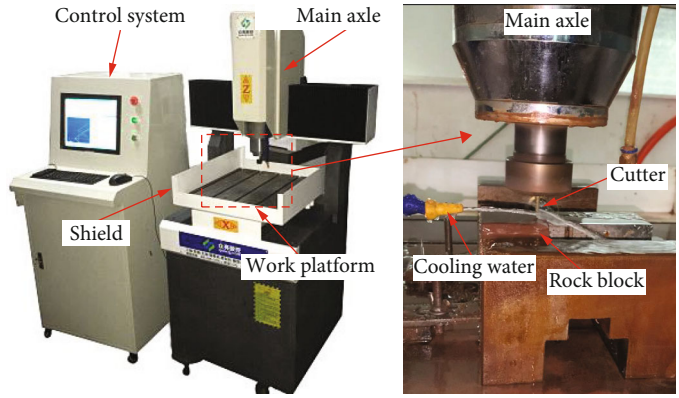

Figure 2: Engraving machine for manufacturing joint specimen.

postprocessing software, namely, JD Paint 5.21 Ultimate, and engraving accuracy was set to 0.1 mm due to precision and time-saving concerns

(2) Carrying out 3D rigid engraving. The engraving paths of the upper and lower joint surfaces were imported into the control system of the 3D engraving machine, respectively. Firstly, the engraving path of the lower joint surface was executed, then the prepared sandstone block was mounted and fixed in the sample fixture, and the cutter was adjusted to the corner of the block surface as the starting point, then the lower joint surface was replicated by cutter and water gun working together along the engraving path. The joint in the upper block was obtained by repeating the above operations. The engraved sandstone joint specimens with three different JRC values are presented in Figure 3

2.4. Roughness Error Analysis of Engraved Joints. To verify the accuracy of joint replicas by the engraving technique, the joint replicas were scanned again by the 3D optical scanner, and the obtained engraved surface data was compared with that of original rock joint. After processing of the points cloud data, the error analysis of the 2D roughness of the original natural joints and the engraved joints was carried out. The point coordinates of the natural and engraved joint surfaces with three different roughnesses at various positions ($X = 10, 20, 30, 40$ mm) were extracted and compared (Figure 4). Comparison of the 2D profile lines between the engraved and original joints showed that they matched each other very well. Moreover, the JRC values of the engraved joint surfaces were further calculated, the obtained JRC values were 1.45, 5.01, and 8.01, respectively, and the JRC errors with the three original joint surfaces were 2.11%, 0.60%, and 0.63%, respectively. The errors between the original and the engraved joints were small and acceptable, and it was evident that the 3D optical scanning coupling with 3D rigid engraving method could duplicate the morphology of the original joint surface exactly onto the engraved joint.

3. Experimental Protocol in Direct Shear Testing

The RMT–150C servo test system was also utilized to perform the direct shear tests on four cubic blocks and joint

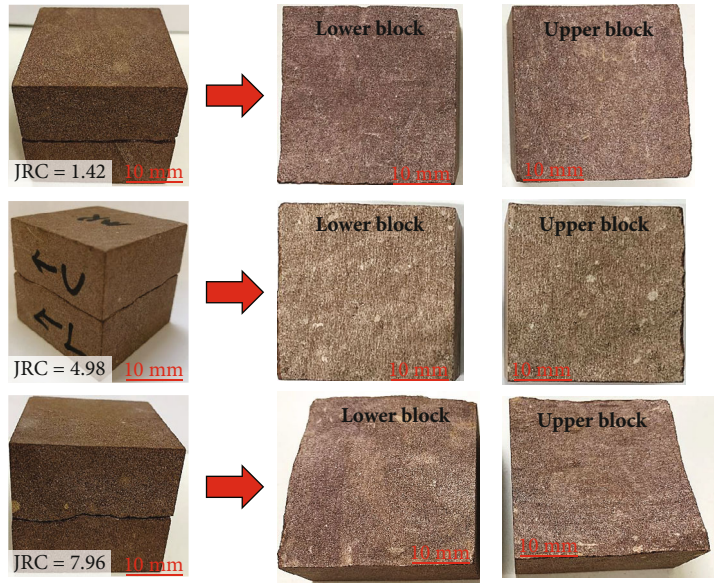

Figure 3: Engraved rock joint specimens of sandstone with natural joint surfaces: column (a) pairs of joint specimens; column (b) lower blocks of joint specimens; column (c) upper blocks of joint specimens.

replicas at different normal stresses at room temperature. Direct shear tests on four cubic blocks with side length of 50 mm were run at normal stresses of 5, 10, 15, and 20 MPa to determine basic friction angle (φ_b) of the studied sandstone. Moreover, two sets of parallel tests were carried out for each roughness of the joint replicas at both normal stresses (i.e., 15 and 30 MPa), in total, twelve sets of engraved joint surfaces were adopted for the shearing measurements. During the tests, the shear direction was parallel to 2D profile lines that were used to calculate JRC values, and the upper and lower blocks were encapsulated in the corresponding shear cells. Each normal stress was applied to the predetermined value by force controlled with the loading rate of 1 kN/s; then, the upper shear cell kept fixed, and the shear force was applied to the lower shear cell in a displacement-controlled manner until the specimen failed at a fixed loading rate of 0.005 mm/s (Figure 5). The fracture development and the failure characteristics of the rock joints under different roughnesses and normal stresses during the shear tests were observed, and the shear stress-displacement curves were recorded. It should be noted that the normal stress was not constant during the shear tests, as the shear displacement increased, the normal stress increased while the apparent contact area between upper and lower joints reduced.

4. Experimental Results

Figure 6 shows shear stress-displacement curves of tested joint replicas with different roughnesses at two normal stresses. In the initial stage before reaching the peak shear strength, all curves generally show a linear increasing trend due to elastic deformation of upper and lower blocks in this period. After reaching about 50% of the peak shear strength, the curves change to increase in a nonlinear way, due to the continuous increase of shear displacement, the asperities of upper and lower blocks begin to fracture and be shorn off by the advance of one block with respect to the other, and the slopes of curves before reaching the peak strength are steeper at 30 MPa than at 15 MPa. After reaching the peak shear strength, the residual strengths of joint replicas at 15 MPa are almost keep steady, while those at 30 MPa are continuously decreasing. The overall trend shows that the strength-weakening is stronger at higher normal stress.

5. Discussion

5.1. Strength Dependence on Surface Roughness. Comparisons of the peak shear strengths between the experimental results and the theoretical values on the basis of the *JRC-JCS* shear strength criterion are made to verify the rationality of shear test results and viability of the sample preparation method. The *JRC-JCS* shear strength criterion is proposed based on direct shear tests of massive natural rock joints, and its detailed expression is written by [16].

$$\tau_n = \sigma_n \tan\left[\mathrm{JRC}\lg\left(\frac{\mathrm{JCS}}{\sigma_n}\right) + \varphi_b\right], \tag{4}$$

where τ_n is the peak shear strength, MPa; σ_n is normal stress, MPa; JRC is the engraved joint roughness coefficient, JCS is the joint wall compressive strength, MPa; and φ_b is the basic friction angle. For the studied sandstone, the rock is fresh and unweathered; hence, it is assumed that JCS = UCS = 95.60 MPa; φ_b is 27° through direct shear test on cubic blocks.

The comparison results are presented in Figure 7. It can be clearly seen that the peak shear stresses with different JCR values are higher at 30 MPa with respect to tests at 15 MPa. However, the shear strength dependence on surface

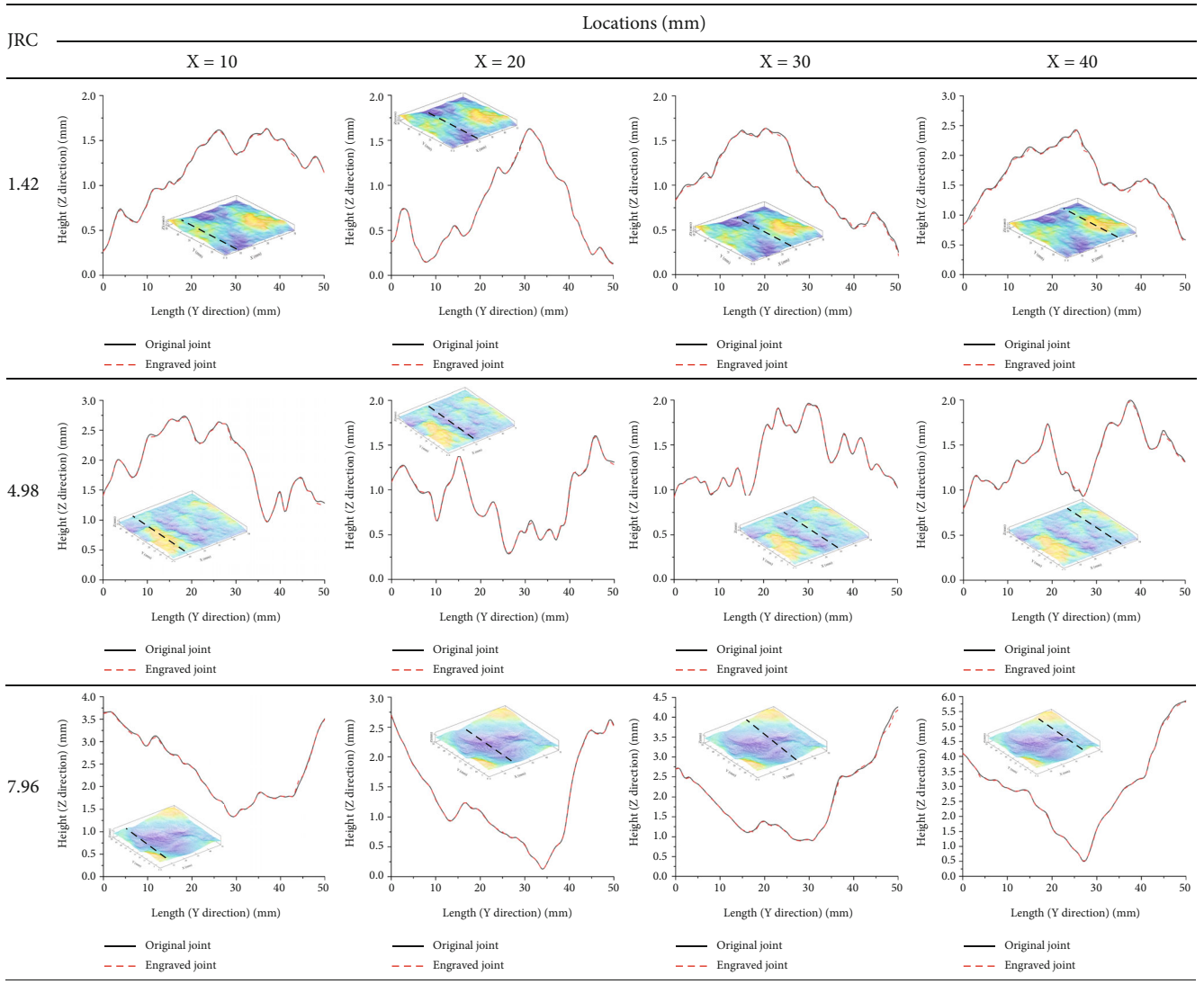

Figure 4: Comparison through 2D profiles at different locations (X) between the original and engraved joints surfaces, where $X = 10, 20, 30, 40$ mm mean profile positions in X direction.

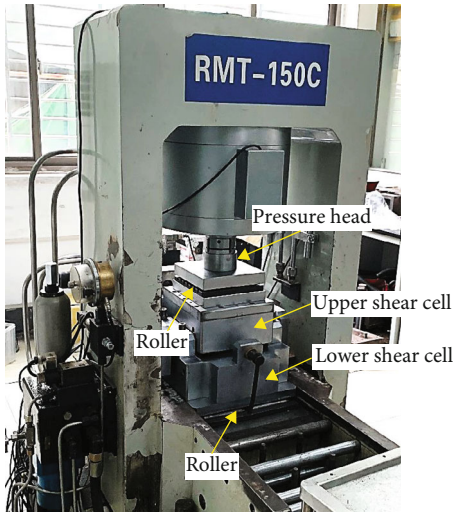

Figure 5: Direct shear test by RMT–150C servo test system.

roughness is similar at both normal stresses. Since the theoretical and experimental peak shear strengths of engraved joints with the same JRC values have small errors (i.e., 4.94%-12.58%) at the same normal stresses; therefore, this result indicates that the obtained experimental data is acceptable and the engraved joint method can be promoted for further study of joint mechanisms.

5.2. Surface Morphology Prior and after Testing. Figures 8 and 9 show the shearing failure process and damage zone (the area surrounded by the yellow lines) of joints with different JRC values at normal stresses of 15 and 30 MPa. The overall failure processes of joints with different roughnesses are similar at different normal stresses. After the shear tests begin, cracks are created at the edges of the upper and lower blocks, and during the continuous shearing process, the cracks continue to expand and new cracks are generated; meanwhile, small rock fragments detach from the outer surface of the blocks, and finally, the upper and lower blocks are

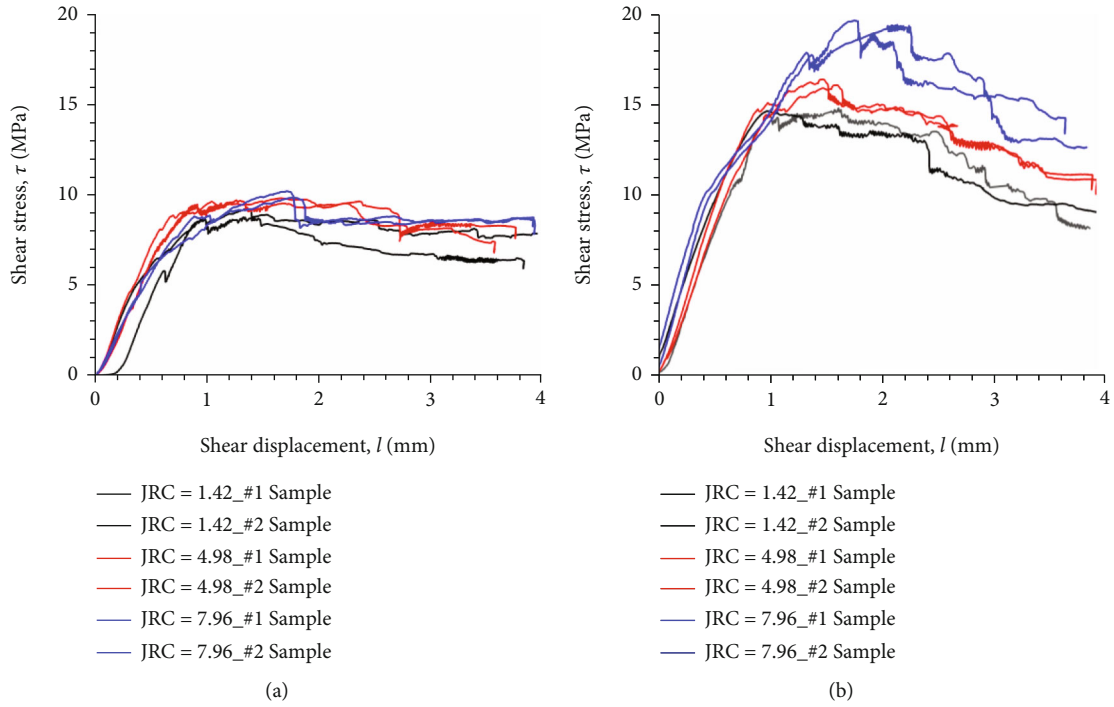

Figure 6: Shear stress-displacement curves of test joint specimens at two normal stresses: (a) 15 MPa; (b) 30 MPa.

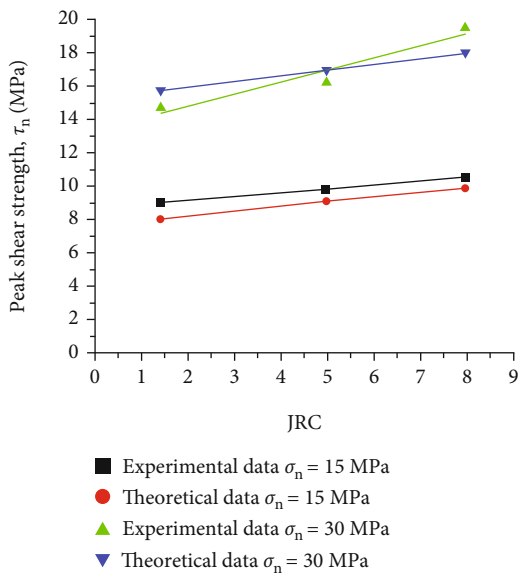

Figure 7: Comparisons of experimental and theoretical peak shear strengths of engraved joints with different JRC values under direct shear tests at two normal stresses.

destroyed, leaving a large amount of gouge on the surface of the specimens. However, at different normal stresses, the resulting surface features are slightly different. In comparisons between Figures 8 and 9, the blocks after the final failure are less damaged at the normal stress of 15 MPa. Furthermore, at the same normal stress, the damage of the joint surface is more severe with the increase of JRC value, and the amount of rock fragments and gouge detaching from blocks continuously increases.

The microscopic morphological features of joint surfaces before and after shear test are shown in Figure 10 by scanning electron microscopy (SEM). Before the shear test, the particles bond together and the surface is very clean (Figure 10(a)), after shear test starts, slipping occurs between the joint surfaces in upper and lower blocks, leading to damage and plucking out of particles, and leaving a large amount of gouge (Figures 10(b) and 10(c)). Moreover, the residual scratches on the surface are the evidence of the grinding of asperities (Figure 10(d)).

5.3. Shearing Mechanism of the Joint Surfaces. The shear behaviors of joints reflect the essence of shearing to some extent, and the shearing mechanism is inevitably affected by normal stress and roughness, which is also confirmed in previous studies [38–40]. The shearing mechanism is affected by the change of roughness, which is reflected by the alteration of the morphology of the asperities during the shearing process at a certain normal stress, and three shearing mechanisms of asperity sliding, asperity surface wear, and asperity shearing off may be observed in direct shear tests at different normal stresses (usually $\sigma_n < 5.0$ MPa) [41], and the patterns of shear strength development depend on different shearing mechanisms. In this study, every joint can be divided into many asperities, which are assumed as sawtooth-shaped units (Figure 11).

When the normal stress σ_1 is low enough, the upper asperity slips along T1 towards the lower asperity (Figure 11(a)), major sliding movement takes place along the joint under this condition, and overall trend of the normal displacement increases in the positive direction (Figure 11(b)). Here, the plus sign in vertical coordinates (i.e., normal displacement) indicates that blocks are

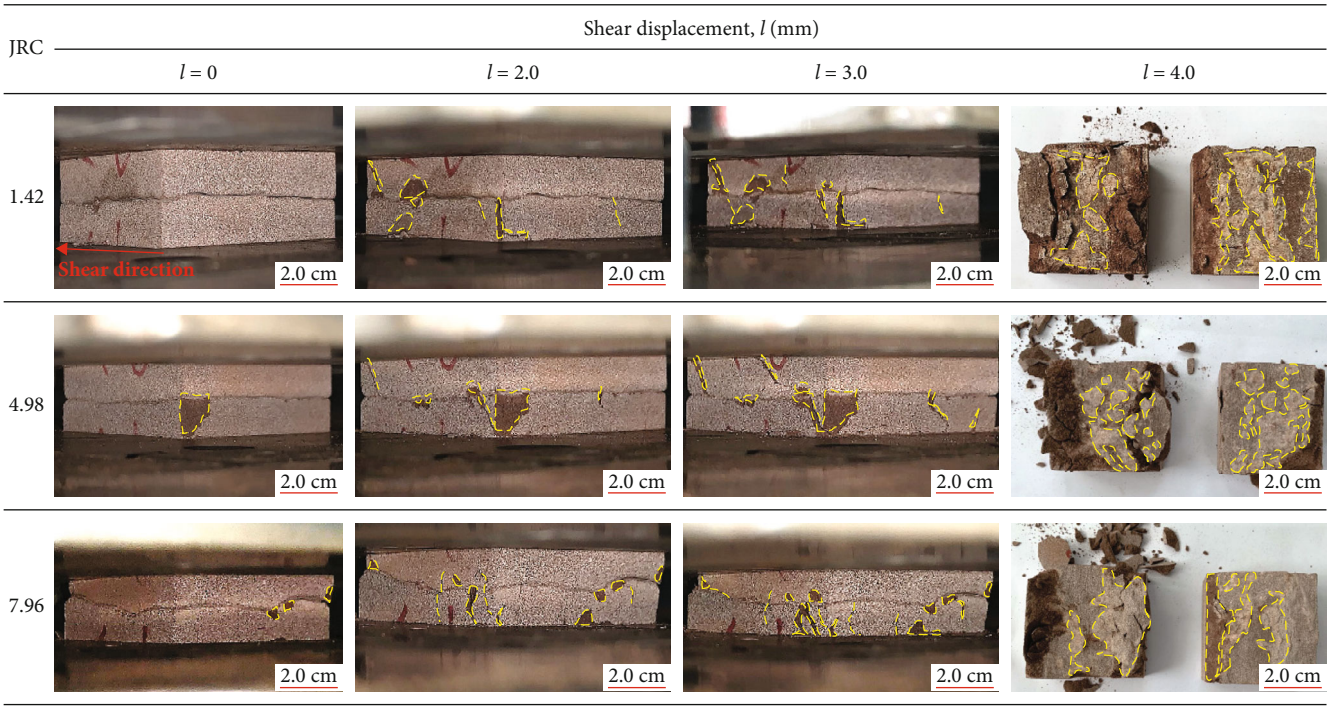

Figure 8: Shear failure process and damage zone of test joint specimens with different JRC values at normal stress of 15 MPa.

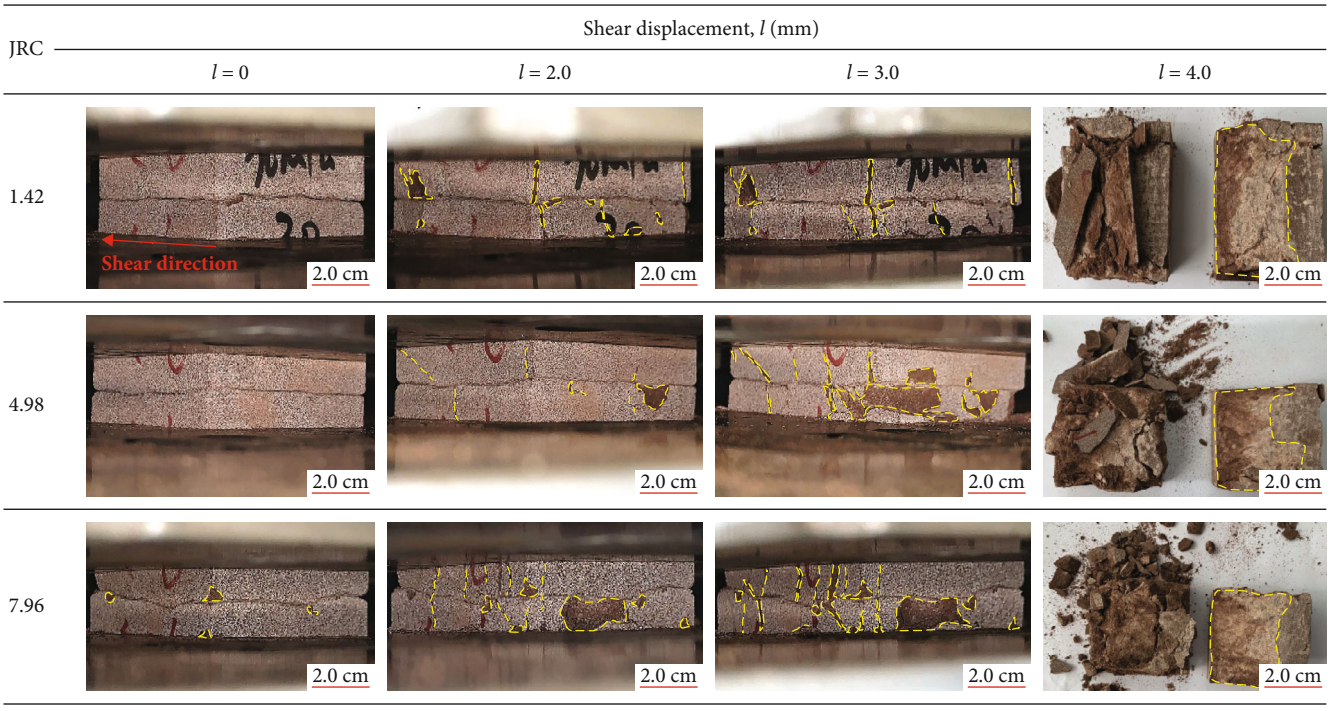

Figure 9: Shear failure process and damage zone of test joint specimens with different JRC values at normal stress of 30 MPa.

departing from each other, while the minus sign in vertical coordinates means that blocks are approaching each other. In this case, the failure zones of joints are primarily caused by asperity sliding wear. When the normal stress σ_2 is sufficiently high, no sliding movement takes place at the asperity, and the asperity is completely shorn off along T2, and the overall trend of normal displacement increases in the negative direction, in this case, the failure zones of joints are mainly induced by shearing of the asperities. When the normal stress σ_3 satisfies $\sigma_1 < \sigma_3 < \sigma_2$, both asperity sliding and shearing off occur, leading to asperity shearing failure along T3, and the overall trend of normal displacement increases

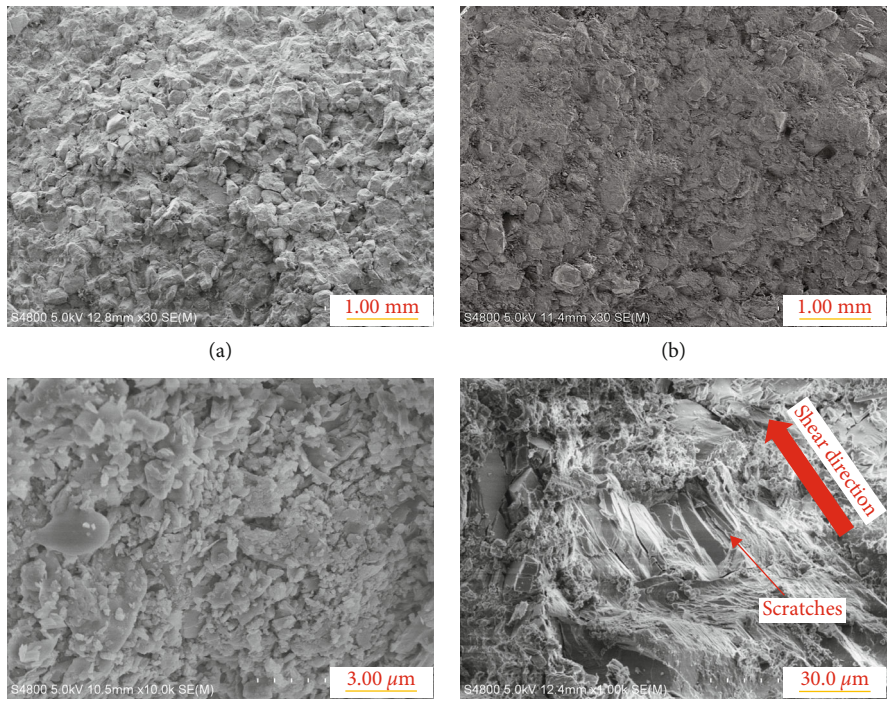

Figure 10: Scanning morphology of joint surface before and after shear tests: (a) and (b) morphological characteristics of the particles before and after shear tests, respectively; (c) and (d) residual gouge and scratches on the shear surfaces, respectively.

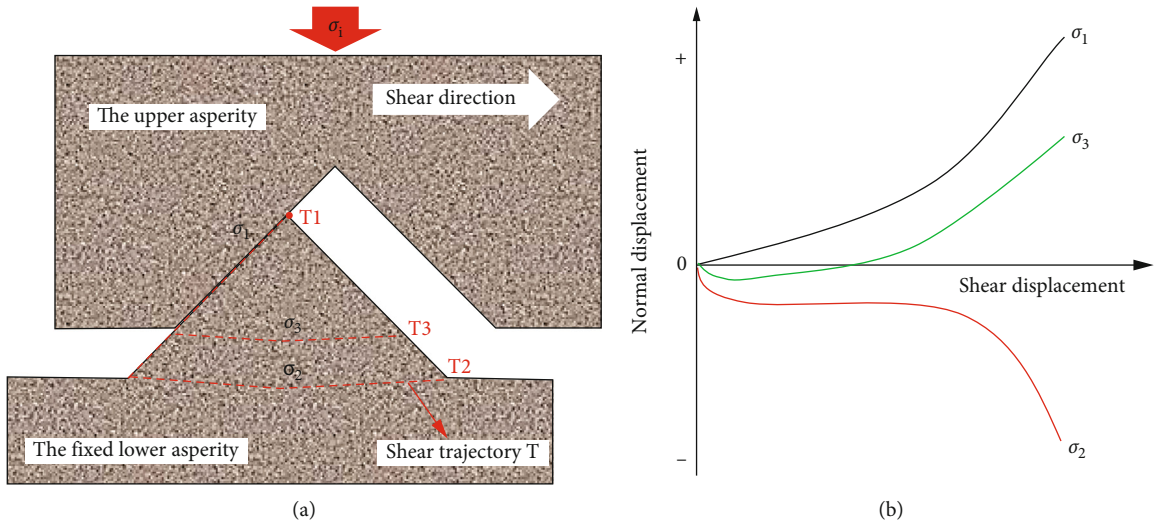

Figure 11: Failure mechanisms of shear behaviors: (a) asperity with the upper and lower blocks; (b) representative shear-normal displacement curves at different normal stresses.

in the positive direction. Therefore, the specific mechanism in this study can be distinguished by the relationship of normal displacement and shear displacement, and the shear-normal displacement curves are shown in Figure 12. During the shearing process, at the initial stage of applying shear force, the blocks are in the volume compression stage, and the downward curves show a nonlinear growth with gradually decreasing slope, and then, the normal displacement does not change significantly, the curves tend to be horizontal, and the asperities are shorn off in this period. With the increasing of shear displacement, a very small amount of gouge between upper and lower joint surfaces is discharged towards lateral sides, and both upper and lower blocks are crazed or even crushed under the combined action of normal and shear forces (Figures 8 and 9, $l = 2.0$, and 3.0 mm), resulting in increased displacement; however, the increase in normal displacement throughout the shearing process at the normal stress of 15 MPa is much lower

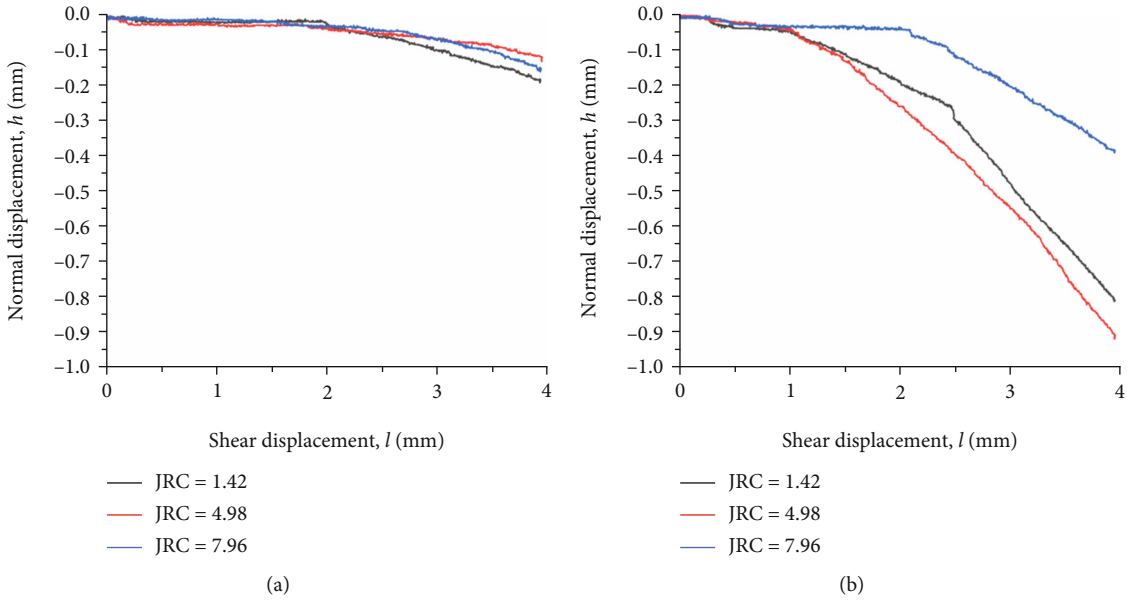

Figure 12: Shear-normal displacement curves at two normal stresses: (a) 15 MPa; (b) 30 MPa.

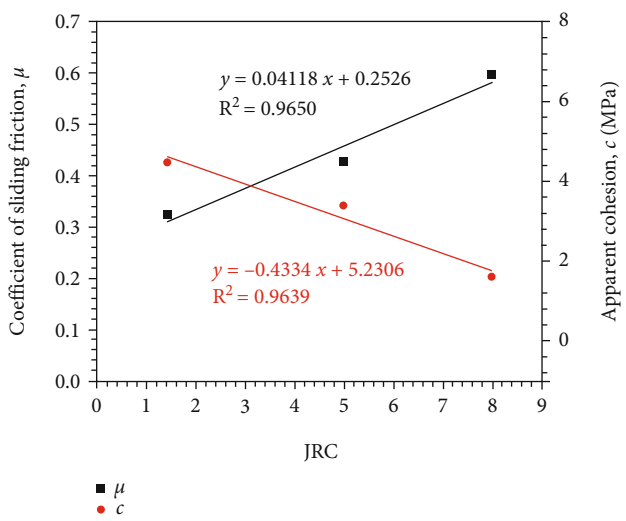

Figure 13: The relationships among JRC value, apparent cohesion, and friction coefficient of test joints.

compared to the case of results at 30 MPa, and there is no dramatic increase (Figure 12(a)), indicating that the upper and lower blocks are slightly damaged. In contrast, the normal displacement is much higher at the normal stress of 30 MPa, and the shear displacements corresponding to the inflection points where the normal displacement increase sharply in Figure 12(b) are exactly where the shear strengths begin to fall in Figure 6(b). In general, the normal displacements continue to increase in the negative direction in Figure 12; therefore, the asperities have not experienced the sliding stage at two applied normal stresses, and the failure mechanism of joints is caused by asperities shearing off, and this finding is similar with those obtained from previous numerical and experimental tests for well-matched joints with the same or different wall strengths under direct shear tests at normal stresses of 3-5 MPa [8, 13, 42].

Although the shearing mechanism of joint surfaces is basically the same at normal stresses of 15 and 30 MPa, however, with the normal stress increases from 15 to 30 MPa, the mechanical behaviors of joints during shearing process are not exactly the same. At normal stress of 15 MPa, most of asperities have an influence and limited number of fracturing occurs on steep-sided roughness features, and the residual strength almost keeps constant. As the normal stress increases to 30 MPa, shearing of almost all asperities occurs, and stress concentration at some asperities results in penetration of tensile cracks inside the intact rock material. Moreover, it is evident that the asperity wearing is more severe on the joint surfaces at the normal stress of 30 MPa (Figures 8 and 9), and the accumulated gouge would compact and spread more evenly along the joint surfaces and subdue the effect of the remaining asperities, besides, cracks on the side of the upper and lower blocks are more developed, leading to residual shear strength continuously decrease.

In engineering practice, for unbonded joints, cohesion is considered as null; however, apparent cohesion, which does not represent a real bond between the rock joint walls, but the imbrication of the roughness at high normal stresses, can also be used for geotechnical engineering projects [26]. In this study, the peak shear strength is composed of the apparent cohesion between the joints (c) and the frictional resistance (F_r) according to the Coulomb-Mohr criterion, the peak shear strength and frictional resistance can be written by

$$\tau_n = c + \sigma_n \tan \varphi_{peak} = c + F_r, \quad (5)$$

$$F_r = \sigma_n \tan \left(\varphi_{peak}\right) = \mu\sigma_n, \quad (6)$$

where μ is the coefficient of sliding friction and φ_{peak} is the friction angle for each joint at peak stage.

Friction coefficient and apparent cohesion are two unknowns for joints with each JRC value, which can be calculated by substituting two normal stresses and the corresponding peak shear strengths into Equations (5) and (6), and Figure 13 shows the relationships among JRC values, friction coefficient, and apparent cohesion at normal stresses of 15 and 30 MPa. It can be seen that roughness characteristics have an effect on apparent cohesion and friction coefficient, a rougher joint leads to a higher friction coefficient, but a lower apparent cohesion. Rullière et al. reported that a rougher joint led to a higher apparent cohesion at the high normal stress (i.e., $\sigma_n \leq 1$ MPa) [26], and they considered that a high normal stress could cause better matching conditions and larger contact points, hence increasing the number of asperities contributing to the apparent cohesion and peak shear strength. However, in this study, apparent cohesions decrease linearly with the increase of JRC values, this may be due to some of the higher asperities are subjected to compression failure in the blocks with JRC of 4.98 and 7.96 at normal stresses of 15 and 30 MPa, leading to the asperities damage in advance, and this will further accelerate the failure of asperities, resulting in the decrease of the apparent cohesion.

6. Conclusions and Prospects

In this paper, 3D optical scanning coupling with 3D rigid engraving was successively employed to fabricate rock joints with the same morphologies as natural joint surfaces. The mass engraving of sandstone showed that the used method had reliable geometric precision and efficient machining ability of joint surface and could provide enough joint samples with the same natural surface for experimental investigation. The direct shear tests were conducted on joint replicas at two high normal load conditions. Based on the above analyses of results and discussion, the following conclusions can be drawn:

(1) The shear strength dependence on surface roughness is similar at normal stresses of 15 and 30 MPa, and the peak shear stresses have a positive correlation with JRC values at normal stresses of 15 and 30 MPa

(2) In this study, at normal stresses of 15 and 30 MPa, the shearing mechanism of joints with different JRC values is asperity shearing off

(3) The friction coefficient of joint surface increases as joint roughness increases, and higher normal loads may lead to a decrease of apparent cohesion, thus weakening the residual strength during the slip

The results of this study facilitate our understanding and reveal the shearing performances and mechanisms of the natural fracture activation behavior during hydraulic fracturing. However, in this study, the shearing properties of natural fractures in deep sandstone reservoir with high temperature and higher pressure (>30 MPa) are not considered. This may induce a different failure mode on the fractures, which will be addressed in our future work.

Data Availability

The data used to support the findings of this study are included within the article and are available from the corresponding author upon request.

Conflicts of Interest

The authors declare that they have no conflicts of interest.

Acknowledgments

This work was supported by the Science and Technology Service Network Initiative of the Chinese Academy of Sciences (Grant No. KFJ-STS-QYZD-174) and National Natural Science Foundation of China (Nos. 52179114 and 52109141). The authors also would like to thank the China National Petroleum Corporation for providing the fund to carry out the study.

References

[1] C. H. Sondergeld, K. E. Newsham, J. T. Comisky, M. C. Rice, and C. S. Rai, "Petrophysical considerations in evaluating and producing shale gas resources," in *SPE Unconventional Gas Conference*, pp. 1–34, Pittsburgh, Pennsylvania, USA, 2010.

[2] R. Rickman, M. Mullen, E. Petre, B. Grieser, and D. Kundert, "A practical use of shale petrophysics for stimulation design optimization: all shale plays are not clones of the Barnett shale," *SPE Annual Technical Conference and Exhibition*, vol. 2, pp. 840–850, 2008.

[3] X. Zhang, B. Wu, R. G. Jeffrey, D. Yang, W. Chen, and F. Zhang, "Changes of slip rate and slip-plane orientation by fault geometrical complexities during fluid injection," *Journal of Geophysical Research - Solid Earth*, vol. 124, no. 8, pp. 9226–9246, 2019.

[4] H. Y. Wang, "Hydraulic fracture propagation in naturally fractured reservoirs: complex fracture or fracture networks," *Journal of Natural Gas Science and Engineering*, vol. 68, article 102911, 2019.

[5] J. A. Rueda Cordero, E. C. Mejia Sanchez, D. Roehl, and L. C. Pereira, "Hydro-mechanical modeling of hydraulic fracture propagation and its interactions with frictional natural fractures," *Computers and Geotechnics*, vol. 111, pp. 290–300, 2019.

[6] N. Barton and S. Bandis, "Some effects of scale on the shear strength of joints," *International Journal of Rock Mechanics and Mining Sciences*, vol. 17, no. 1, pp. 69–73, 1980.

[7] M. Gencer, "Progressive failure in stratified and jointed rock mass," *Rock Mechanics and Rock Engineering*, vol. 18, no. 4, pp. 267–292, 1985.

[8] Y. Li, H. Zhou, W. Zhu, S. Li, and J. Liu, "Experimental and numerical investigations on the shear behavior of a jointed rock mass," *Geosciences Journal*, vol. 20, no. 3, pp. 371–379, 2016.

[9] A. El-Naqa, "A comparative review in regards to estimating bearing capacity in jointed rock masses in northeast Jordan," *Bulletin of Engineering Geology and the Environment*, vol. 63, no. 3, pp. 233–245, 2004.

[10] J. Byerlee, "Frictional characteristics of granite under High confining pressure," *Journal of Geophysical Research*, vol. 72, no. 14, pp. 3639–3648, 1967.

[11] M. Singh, K. S. Rao, and T. Ramamurthy, "Strength and deformational behaviour of a jointed rock mass," *Rock Mechanics and Rock Engineering*, vol. 35, no. 1, pp. 45–64, 2002.

[12] M. K. Elmouttie, G. V. Poropat, and A. G. Meyers, "Quantifying the significance of isotropic joints in structural analysis," *Computers and Geotechnics*, vol. 42, pp. 21–36, 2012.

[13] M. Bahaaddini, G. Sharrock, and B. K. Hebblewhite, "Numerical direct shear tests to model the shear behaviour of rock joints," *Computers and Geotechnics*, vol. 51, pp. 101–115, 2013.

[14] A. Usefzadeh, H. Yousefzadeh, H. Salari-Rad, and M. Sharifzadeh, "Empirical and mathematical formulation of the shear behavior of rock joints," *Engineering Geology*, vol. 164, pp. 243–252, 2013.

[15] Q. Jiang, B. Yang, F. Yan, C. Liu, Y. Shi, and L. Li, "New method for characterizing the shear damage of natural rock joint based on 3D engraving and 3D scanning," *International Journal of Geomechanics*, vol. 20, no. 2, article 06019022, 2020.

[16] N. Barton and V. Choubey, "The shear strength of rock joints in theory and practice," *Rock Mechanics*, vol. 10, no. 1-2, pp. 1–54, 1977.

[17] B. K. Fifer, "Determining the surface roughness coefficient by 3D scanner," *Geologija*, vol. 53, no. 2, pp. 147–152, 2010.

[18] B. S. A. Tatone and G. Grasselli, "A new 2D discontinuity roughness parameter and its correlation with JRC," *International Journal of Rock Mechanics and Mining Sciences*, vol. 47, no. 8, pp. 1391–1400, 2010.

[19] R. Tse and D. M. Cruden, "Estimating joint roughness coefficients," *International Journal of Rock Mechanics and Mining Sciences*, vol. 16, no. 5, pp. 303–307, 1979.

[20] P. H. S. W. Kulatilake, P. Balasingam, J. Park, and R. Morgan, "Natural rock joint roughness quantification through fractal techniques," *Geotechnical and Geological Engineering*, vol. 24, no. 5, pp. 1181–1202, 2006.

[21] Y. H. Lee, J. R. Carr, D. J. Barr, and C. J. Haas, "The fractal dimension as a measure of the roughness of rock discontinuity profiles," *International Journal of Rock Mechanics and Mining Sciences*, vol. 27, no. 6, pp. 453–464, 1990.

[22] Y. Zhao, C. Wang, L. Ning, H. Zhao, and J. Bi, "Pore and fracture development in coal under stress conditions based on nuclear magnetic resonance and fractal theory," *Fuel*, vol. 309, article 122112, 2022.

[23] Y. Zhao, C. L. Wang, and J. Bi, "Analysis of fractured rock permeability evolution under unloading conditions by the model of elastoplastic contact between rough surfaces," *Rock Mechanics and Rock Engineering*, vol. 53, no. 12, pp. 5795–5808, 2020.

[24] Y. Chen, H. Lin, X. Ding, and S. Xie, "Scale effect of shear mechanical properties of non-penetrating horizontal rock-like joints," *Environment and Earth Science*, vol. 80, no. 5, pp. 1–10, 2021.

[25] X. Zhang, H. Lin, Y. Wang, R. Yong, Y. Zhao, and S. Du, "Damage evolution characteristics of saw-tooth joint under shear creep condition," *International Journal of Damage Mechanics*, vol. 30, no. 3, pp. 453–480, 2021.

[26] A. Rullière, P. Rivard, L. Peyras, and P. Breul, "Influence of roughness on the apparent cohesion of rock joints at low normal stresses," *Journal of Geotechnical and Geoenvironmental Engineering*, vol. 146, no. 3, article 04020003, 2020.

[27] B. Indraratna, S. Thirukumaran, E. T. Brown, W. Premadasa, and W. Gale, "A technique for three-dimensional characterisation of asperity deformation on the surface of sheared rock joints," *International Journal of Rock Mechanics and Mining Sciences*, vol. 70, pp. 483–495, 2014.

[28] C. C. Xia, Z. C. Tang, W. M. Xiao, and Y. L. Song, "New peak shear strength criterion of rock joints based on quantified surface description," *Rock Mechanics and Rock Engineering*, vol. 47, no. 2, pp. 387–400, 2014.

[29] Y. Zhao, L. Zhang, W. Wang, Q. Liu, L. Tang, and G. Cheng, "Experimental study on shear behavior and a revised shear strength model for infilled rock joints," *International Journal of Geomechanics*, vol. 20, no. 9, article 04020141, 2020.

[30] Y. Zhao, L. Zhang, W. Wang, J. Tang, H. Lin, and W. Wan, "Transient pulse test and morphological analysis of single rock fractures," *International Journal of Rock Mechanics and Mining Sciences*, vol. 91, pp. 139–154, 2017.

[31] R. M. Roosta, M. H. Sadaghiani, A. Pak, and Y. Saleh, "Rock joint modeling using a visco-plastic multilaminate model at constant normal load condition," *Geotechnical and Geological Engineering*, vol. 24, no. 5, pp. 1449–1468, 2006.

[32] E. S. Hong, I. M. Lee, G. C. Cho, and S. W. Lee, "New approach to quantifying rock joint roughness based on roughness mobilization characteristics," *KSCE Journal of Civil Engineering*, vol. 18, no. 4, pp. 984–991, 2014.

[33] K. Amiri Hossaini, N. Babanouri, and N. S. Karimi, "The influence of asperity deformability on the mechanical behavior of rock joints," *International Journal of Rock Mechanics and Mining Sciences*, vol. 70, pp. 154–161, 2014.

[34] H. Atapour and M. Moosavi, "The influence of shearing velocity on shear behavior of artificial joints," *Rock Mechanics and Rock Engineering*, vol. 47, no. 5, pp. 1745–1761, 2014.

[35] C. W. A. Harbord, S. B. Nielsen, N. De Paola, and R. E. Holdsworth, "Earthquake nucleation on rough faults," *Geology*, vol. 45, no. 10, pp. 931–934, 2017.

[36] E. E. Brodsky, J. D. Kirkpatrick, and T. Candela, "Constraints from fault roughness on the scale-dependent strength of rocks," *Geology*, vol. 44, no. 1, pp. 19–22, 2016.

[37] Q. Jiang, X. Feng, Y. Gong, L. Song, S. Ran, and J. Cui, "Reverse modelling of natural rock joints using 3D scanning and 3D printing," *Computers and Geotechnics*, vol. 73, pp. 210–220, 2016.

[38] M. C. Weng, F. S. Ã. Jeng, T. H. Huang, and M. L. Lin, "Characterizing the deformation behavior of Tertiary sandstones," *Characterizing the Deformation Behavior of Tertiary Sandstones*, vol. 42, no. 3, pp. 388–401, 2005.

[39] Y. Lu, L. Wang, Z. Li, and H. Sun, "Experimental study on the shear behavior of regular sandstone joints filled with cement grout," *Rock Mechanics and Rock Engineering*, vol. 50, no. 5, pp. 1321–1336, 2017.

[40] M. Bahaaddini, P. C. Hagan, R. Mitra, and B. K. Hebblewhite, "Parametric study of smooth joint parameters on the shear behaviour of rock joints," *Rock Mechanics and Rock Engineering*, vol. 48, no. 3, pp. 923–940, 2015.

[41] Y. Li, L. Song, Q. Jiang, C. Yang, C. Liu, and B. Yang, "Shearing performance of natural matched joints with different wall strengths under direct shearing tests," *Geotechnical Testing Journal*, vol. 41, no. 2, pp. 371–389, 2018.

[42] X. Zhang, Q. Jiang, N. Chen, W. Wei, and X. Feng, "Laboratory investigation on shear behavior of rock joints and a new peak shear strength criterion," *Rock Mechanics and Rock Engineering*, vol. 49, no. 9, pp. 3495–3512, 2016.